Process Safety and Environmental Protection 186 (2024) 1169–1182

Contents lists available at ScienceDirect

Process Safety and Environmental Protection

journal homepage: www.journals.elsevier.com/process-safety-and-environmental-protection

Modeling the performance of multilayer insulation in cryogenic tanks undergoing external fire scenarios

Davide Camplese [a], Giordano Emrys Scarponi [a], Carmela Chianese [a], Aliasghar Hajhariri [b], Robert Eberwein [b], Frank Otremba [b], Valerio Cozzani [a,*]

[a] LISES - Laboratory of Industrial Safety and Environmental Sustainability - Department of Civil, Chemical, Environmental and Material Engineering, University of Bologna, via Terracini 28, Bologna 40131, Italy
[b] BAM – Department of Tanks for the Storage of Dangerous Goods and Accident Mechanics, Unter den Eichen 87, Berlin 12205, Germany

ARTICLE INFO

Keywords:
Multilayer Insulation
Cryogenic Vessels
Liquefied Hydrogen Storage
Hydrogen Safety
Fire Scenarios

ABSTRACT

Multilayer Insulation (MLI) is frequently used in vacuum conditions for the thermal insulation of cryogenic storage tanks. The severe consequences of the degradation of such materials in engulfing fire scenarios were recently evidenced by several large-scale experimental tests. In the present study, an innovative modelling approach was developed to assess the performance of heat transfer in polyester-based MLI materials for cryogenic applications under fire conditions. A specific layer-by-layer approach was integrated with an apparent kinetic thermal degradation model based on thermogravimetric analysis results. The modeling results provided a realistic simulation of the experimental data obtained by High-Temperature Thermal Vacuum Chamber tests reproducing fire exposure conditions. The model was then applied to assess the behavior of MLI systems for liquid hydrogen tanks in realistic fire scenarios. The results show that in intense fire scenarios degradation occurs rapidly, compromising the thermal insulation performances of the system within a few minutes.

1. Introduction

In the ongoing energy transition scenario, hydrogen is emerging as a promising alternative energy carrier having a low environmental impact, while the use of natural gas is currently proposed as an alternative to other fossil fuels to reduce greenhouse gas emissions (Preuster et al., 2017; Speirs et al., 2019).

The storage and transportation of these substances as liquids in cryogenic tanks, e.g. in the form of liquefied natural gas (LNG) and liquefied hydrogen (LH_2), appears to be among the most effective solutions to achieve high volumetric energy density (Kunze and Kircher, 2012). Since maintaining cryogenic conditions as well as low boil-off rates for prolonged periods is crucial, heat leakage into cryogenic tanks must be minimized. For this purpose, thermal superinsulation systems such as vacuum combined with perlite, microspheres, or Multilayer Insulation (MLI) have been developed. In particular, nowadays systems with MLI have the smallest volume requirement and lowest weight (Edward and Filip, 2018). These features are of great importance in the transportation sector, where space and weight constraints play a crucial role.

Besides the advantages associated with the widespread deployment of LNG and LH_2 new technologies, there are also significant hazards to consider due to the high flammability of these substances (Dan et al., 2014; Eberwein, 2021; Iannaccone et al., 2019; Sánchez and Williams, 2014). An accidental loss of integrity of LNG and LH_2 cryogenic storage units might result in extremely dangerous phenomena, such as Boiling Liquid Expanding Vapour Explosion (BLEVE) (Abbasi and Abbasi, 2007; van Wingerden et al., 2022b) and Fireballs (Zalosh and Weyandt, 2005). Release of cryogenic liquids as LNG over water may result in Rapid Phase Transition (Aursand and Hammer, 2018; Brown et al., 1990), although the occurrence of such a phenomenon was recently excluded in a recent study by (van Wingerden et al., 2022a) addressing LH_2. In this framework, tank integrity may be jeopardized by exposure to an external heat source such as a fire triggered by a road accident. Despite the presence of thermal superinsulation systems, the results of real-scale fire tests have shown that tanks for the storage of cryogenic fluids can fail in such a scenario (Pehr, 1996; van Wingerden et al., 2022b). Concerning tanks equipped with MLI, a recent study by Eberwein et al. (2023) confirmed that tank failure is due to the thermal degradation of MLI exposed to high temperatures, which leaves the tank unprotected from the fire heat flux. As a result, the tank lading undergoes rapid

* Corresponding author.
E-mail address: valerio.cozzani@unibo.it (V. Cozzani).

https://doi.org/10.1016/j.psep.2024.04.061
Received 13 December 2023; Received in revised form 18 March 2024; Accepted 14 April 2024
Available online 18 April 2024

Nomenclature

T	temperature, K
N	number of radiative layers, -
c_p	specific heat capacity at constant pressure, J/(kg·K)
h	convective heat transfer coefficient, W/(m^2·K)
Nu	Nusselt number, -
Gr	Grashof number, -
Pr	Prandtl number, -
Ra	Rayleigh number, -
H	longitudinal characteristic length of the vacuum enclosure, m
R	universal gas constant, J/(mol·K)
ρ	density, kg/m^3
δ	thickness, m
k	thermal conductivity, W/(m·K)
g	gravitational acceleration, m^2/s
α	coefficient of volume expansion, K^{-1}
μ	dynamic viscosity, Pa·s
ν	kinematic viscosity, m^2/s
q	heat flux, kW/m^2
M	molecular weight, kg/mol
ζ	atomic degrees of freedom of the gas (it equals 2 for air and nitrogen), -
θ	accommodation factor, -
σ	Stefan-Boltzmann coefficient, W/(m^2·K^4)
C_2	empirical constant for the spacer material, -
f	relative density of the spacer to the solid spacer material, -
P	residual gas pressure within the spacer, Pa
ε	emissivity of the material surface, -
D_x	actual thickness of the spacer, m
m	mass, kg
t	time, s
Y_s	solid mass at instant t normalized on the initial value, -
n	reaction order, -
A	preexponential factor, 1/s
E_a	activation energy, J/mol
β	heating rate, °C/min Q
Q	heat power, kW
A_t	total area of the MLI sample tested at the HTTVC (0.042 m^2), m^2
A_d	MLI sample area affected by thermal degradation in the HTTVC test (0.021 m^2), m^2
t_{td}	total degradation time, min

Acronyms

MLI	Multilayer Insulation
LNG	Liquefied Natural Gas
LH_2	Liquefied Hydrogen
CFD	Computational Fluid Dynamics
HTTVC	High-Temperature Thermal Vacuum Camera
TG	Thermogravimetric
VCS	Vapor-Cooled Shield

Subscripts and superscripts

rl	radiative layer
Se	external shell
Si	internal shell
N	outermost radiative layer
i	layer number
1	innermost radiative layer
L	liquid
f	fire
s	solid
g	gas
exp	experimental
0	initial condition

pressurization, which can induce catastrophic failure.

Understanding the mechanism of degradation and the behavior of the cryogenic fluid during fire scenarios is of paramount importance to understand the overall response of a tank exposed to a fire, as well as to ensure a safe tank design and to support emergency response planning.

Numerical models validated by accurate experiments are particularly suitable for this concern. Several Computational Fluid Dynamics (CFD) models (D'Aulisa et al., 2014; Hadjisophocleous et al., 1990; Scarponi et al., 2019) and zone models (Berge, 2009; Johnson, 1998a, 1998b; Landucci et al., 2009) are available in the literature to predict the response of atmospheric and pressure tanks exposed to fire, which provide results in acceptable agreement with fire test data.

Recently, several researchers devoted their efforts to extending such models to cryogenic tanks. Scarponi et al. (2016), Hulsbosch-Dam et al. (2017), and Ustolin et al. (2021) proposed lumped approaches to simulate the pressure build-up and temperature behavior of LNG and LH_2 tanks under fire attack. Iannaccone et al. (2021) developed a 2D CFD model to predict the response of LNG cryogenic tanks exposed to high heat loads such as those induced by fire. A similar CFD study was carried out to simulate an LH_2 vessel by Ustolin et al. (2022). In both studies predictions in line with experimental observations could only be achieved by fine-tuning the insulation system (perlite, polyurethane foam, MLI) equivalent thermal conductivity, empirically setting it to higher values than those measured in normal operating conditions. Thus, due to the lack of a model able to simulate the behaviour of superinsulation systems during exposure to intense fire, the applicability of the above-mentioned approaches is limited to the specific tank considered.

When considering the general performance of MLI systems, several studies are available in the literature proposing models to predict the heat flux and temperature profile both in steady state (Bapat et al., 1990; McIntosh, 1994) and transient regimes (Ji et al., 2014; Jiang et al., 2021). An extensive review of such models is provided by Sutheesh and Chollackal (2018). Nevertheless, to the knowledge of the authors, the available models are focused on normal operating conditions, and can not be used to predict the MLI insulation performance in case of fire exposure.

The aim of this study is to develop an innovative heat transfer model for polyester-based MLI considering the degradation phenomena occurring at high temperatures based on a specific investigation of the MLI behaviour. For this purpose, thermogravimetric (TG) runs were carried out on the MLI to assess the material thermal stability and weight loss at high temperatures. Based on the TG results, a model that simulates the apparent kinetic of MLI thermal degradation was developed and integrated into the "layer by layer" approach proposed by McIntosh (1994).

Thus, the original approach developed in the present study represents a novelty in the panorama of the models for the evaluation of the performance of MLI systems, none of which is able to reproduce the MLI degradation under fire conditions. The modeling results were compared with the bench-scale experimental data presented by Eberwein et al. (2023), obtained in fire-like conditions. The model was then applied to simulate the performance of a full-scale polyester-based MLI system for liquid hydrogen cryogenic vessels during fire exposure, considering four different scenarios based on standard fire curves. The results of the case studies as well as the evidence collected during the experiments

highlight the importance of accounting for MLI degradation phenomena in the analysis of the insulation performance in high-temperature conditions. The innovative approach proposed in this study thus paves the way for the development of improved tools aiming at the assessment of cryogenic tank behavior in fire accident scenarios. The model developed may, in perspective, be integrated into both CFD and lumped modelling approaches for the calculation of the time to failure of cryogenic equipment in the presence of external fires, overcoming the limitations inherent to the empirical fine-tuning of the insulation thermal conductivity adopted by several authors (Iannaccone et al., 2021; Ustolin et al., 2022).

2. Overview of the methodological approach

An innovative approach was developed to assess the performance of polyester-based MLI thermal insulations in the presence of external fires. The methodology is based on three main steps, as shown in Fig. 1: i) experimental tests; ii) definition and validation of a heat transfer model considering the MLI thermal degradation kinetics; and, iii) application of the model to the analysis of case studies considering reference fire scenarios.

The first step is articulated into two different experimental campaigns: the thermogravimetric (TG) analysis (described in Section 3.2), where data on the kinetic of MLI thermal degradation were collected, and the testing of MLI using an in-house bench scale apparatus (described in Section 3.3), called the High-Temperature Thermal Vacuum Chamber (HTTVC), that simulates the fire exposure of the MLI system in conditions reproducing typically present in cryogenic tanks.

In the second step of the methodology, the outcome of the TG analysis is used to define an apparent kinetic model for the degradation of polyester-based MLI. This is then integrated into a heat transfer model, which is validated against the HTTVC test results.

The last step consists of the definition of case studies considering different standard fire curves and the application of the heat transfer model to simulate the response of a full-scale polyester-based MLI system for liquid hydrogen cryogenic vessels in fire scenarios.

3. Experimental section

3.1. Materials

Commercial Polyester-based MLI was used in all experimental tests. The MLI samples analyzed (Fig. 2) consisted of 10 radiative layers of 12 μm thick polyester foils coated with pure aluminium on each side (coating thickness = 40 nm), alternated with layers of non-woven pure polyester material without binders. The overall MLI system (radiative layers + spacers) has a nominal area weight of 0.308 kg/m^2. The material properties relevant for modeling the heat transfer are reported in Table 1.

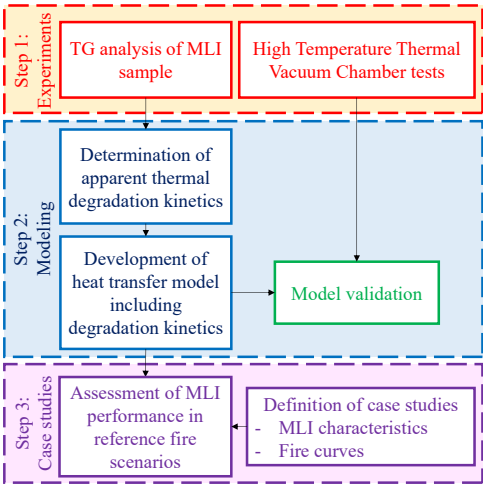

Fig. 1. Flowchart of the methodology.

Fig. 2. An image of the tested MLI showing the alternated spacer and radiative layers.

3.2. Thermogravimetric analysis

Thermal stability and weight loss of MLI samples were investigated using a TG analyser (*TGA-Q500, TA Instruments-Water, USA*).

TG tests were carried out on MLI samples of approximately 10 mg. The sample was cut from the starting material, compressed, and positioned on a copper crucible.

Experimental runs were performed on samples of the whole MLI (i.e., radiative layers + spacers), on the polyester spacer, and on the radiative aluminium layer. The temperature program consisted of three steps: a 30 min isotherm at 30 °C (to stabilize the sample), a linear temperature ramp from 30 °C to 900 °C, and a 10 min isotherm at 900 °C. Three different heating rates were considered for the temperature ramp:10 °C/min, 20 °C/min, and 45 °C/min. An overall flow rate of 100 mL/min was continuously supplied to the apparatus throughout the experimental tests. Depending on the aim of the test, either pure nitrogen (N_2) or dry air was supplied to the sample. The results of the TG tests reported in Section 5.1 show the average data obtained from the three runs.

3.3. High-temperature thermal vacuum chamber (HTTVC) tests

The benchmark for the validation of the proposed MLI thermal degradation model is the experimental tests carried out by Eberwein et al. (2023). The tests were performed in an in-house built device, the HTTVC, aimed at testing MLI and similar insulation material under simulated fire conditions.

The HTTVC is a 600 mm high steel cylinder with an outer diameter of 320 mm. Fig. 3 schematizes the vertical section of the device. The MLI is positioned on a circular sample carrier inside the test chamber, with an opening area of 0.042 m^2, between the bottom wall of the HTTVC and an austenitic-steel-coated copper plate, both of which are coated with thin austenitic steel plates (AISI 316 L) on the sides facing the MLI sample. The top of the copper plate is in direct contact with a coiled tube heat exchanger using water as the cold fluid. The water flow rate as well as the inlet and outlet water temperature are measured. Thus, the heat flux entering the cooling fluid can be calculated applying a (transient) thermal balance on the water stream flowing through the heat exchanger. The heat exchanger surfaces not in contact with the copper

Table 1
Material properties of the MLI sample considered in the model.

Material	Property	Symbol	Value	Unit	Source
Aluminium-polyester radiative layer	Number of layers	N	10	-	MLI datasheet
	Thickness	$\delta_{rl,0}$	$1.2{\cdot}10^{-5}$	m	MLI datasheet
	Specific heat capacity	$c_{p,rl}$	1000	J/(kg·K)	(Van der Vegt and Govaert, 2003)
	Density	ρ_{rl}	1380	kg/m^3	Average among the values reported in (Bamford and Jenkins, 1955)
	Emissivity	ε_i	0.04	-	Highest (most conservative) value among those proposed in the literature (Huang et al., 2017; Jiang et al., 2021; Wang et al., 2016)
Polyester spacer	Relative density of the spacer to the solid material	f_0	0.0358	-	-
	Spacer thickness	D_x	$2.88{\cdot}10^{-4}$	m	-
	Thermal conductivity of the solid spacer material	k_s	0.195	W/(m·K)	(Speight, 2005; Van der Vegt and Govaert, 2003)
	Empirical constant	C_2	0.008	-	(McIntosh, 1994)
	Accommodation coefficient	θ	0.9	-	(Corruccini, 1959)
	Specific heat ratio	γ	1.4	-	(NIST, 2019)

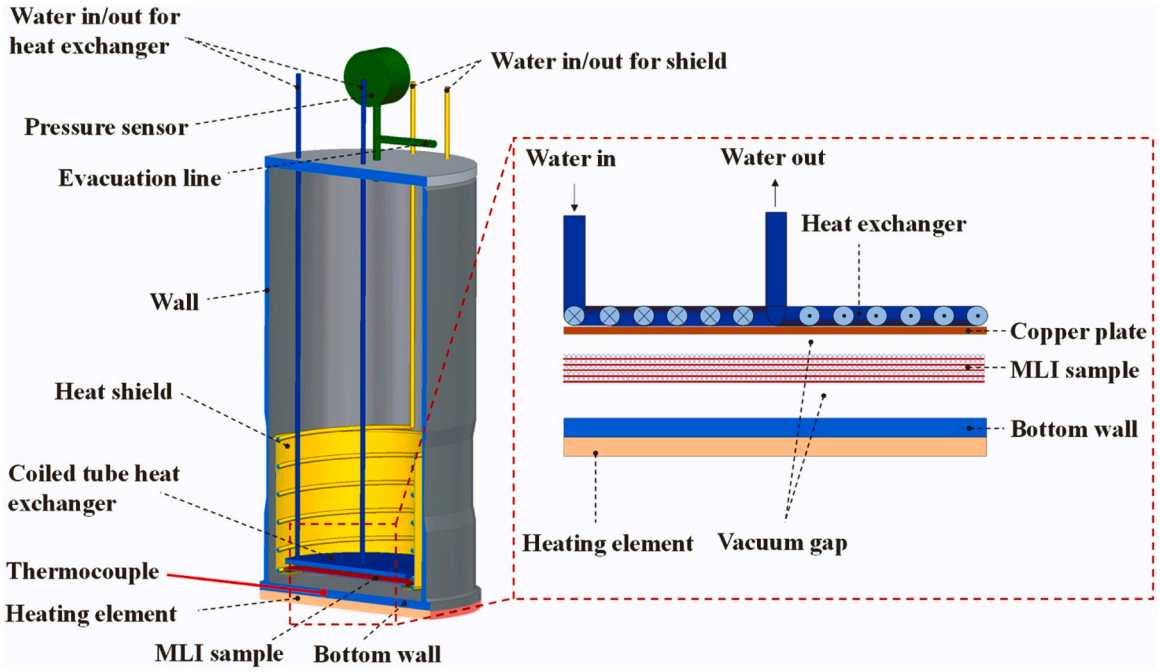

Fig. 3. Frontal section of the HTTVC.

plate are wrapped in superinsulation materials and a water-cooled heat shield surrounds the MLI sample and the heat exchanger to minimize the heat transfer to the surroundings. The heat shield has a flat bottom with a circular opening identical to the surface area of the sample with the function of holding the sample carrier and limiting the cross-sectional area of the MLI exposed to the heat source. Two heating mats connected to an inverter are positioned in direct contact with the bottom wall and used as the heating elements of the system. These can provide a heat flow of up to 100 kW/m^2. A thermocouple is used to measure the temperature of the bottom wall during the test. Preliminary runs on the apparatus without the MLI sample demonstrated that the heat dispersions are negligible and that the heat flow to the water flowing through the heat exchanger provides a reliable measure of the net heat flow from the bottom wall to the copper plate. The MLI material tested is the same used in the TG runs (see Section 3.2) and is described in Section 3.1. Further details on the experimental device and the measurement procedure are available elsewhere (Eberwein et al., 2023).

Before the beginning of each test, the polyester-based MLI sample (see Section 3.1) is positioned in the chamber and a single-level vacuum pump is connected to the evacuation line shown in Fig. 3. The pump is activated to reduce the pressure down to 300 Pa before the start of the experimental run. The pump is then turned off and the heating system of the bottom wall of the HTTVC is started. Two different tests were carried out, varying the maximum temperature of the bottom wall.

In the first test, referred to as TEST #1, the bottom wall is heated from ambient temperature (4 °C) to 750 °C using a heating rate of 20 °C/min, then is maintained isothermal at the final temperature for 30 minutes. Finally, the HTTVC is cooled down for about 40 minutes replacing the heating mats with a water-cooled heat exchanger.

A second test, referred to as TEST #2, was performed with the same heating program but reaching a higher temperature of the bottom wall (770 °C).

4. Modelling

4.1. MLI heat transfer and degradation model

A MLI system consists of several layers of low-emissivity material (radiative layers), typically aluminium or aluminium-coated polyester, interleaved with low thermal conductivity spacers to avoid direct contact between the radiative layers. Cryogenic tanks featuring MLI thermal insulation are double-walled vessels. The MLI is installed in the gap

between the two vessel shells and is typically wrapped around the inner shell, leaving a vacuum gap on the other side. High-vacuum conditions are then applied. Assuming that the vessel characteristic dimension (e.g., the diameter in the case of bullet tanks) is much bigger than the gap between the two vessel shells, a planar geometry may be used to provide a representative simulation of the heat transfer through the MLI.

The MLI thermal degradation model presented in this study schematizes the tank walls and insulation system structure in N+2 nodes, as shown in Fig. 4. Table 2 reports the model equations.

Since the density of the radiation layer is higher than that of the spacer material, the mass and the heat capacity of the spacers are neglected in accordance with other MLI heat transfer models available in the literature (e.g., Jiang et al., 2021; McIntosh, 1994).

Thus, a thermal node is assigned to each one of the *N* radiative layers. The last two nodes, S_i and S_e, are representatives of the internal and external shells, respectively. The transient thermal heat balance equation is written for each node (Eqs. 1–5 in Table 2). Assuming uniform boundary conditions on both internal and external shells and disregarding the edge effects, a temperature gradient is considered to exist only in the direction normal to the surface of the layer. This results in a one-dimensional approach. The effect of curvature is neglected.

In Table 2, Eqs. 2–4 express the thermal balances for the MLI radiative layers, where $\delta_{rl,i}$, $c_{p,rl}$, and ρ_{rl} represent respectively the thickness, the specific heat capacity, and the density of the radiative layer. The subscript *i* refers to the i^{th} radiative layer. Eq. 3 is applied to all the radiative layers except for the outermost and the innermost ones. $q_{rl,i+1}$ and $q_{rl,i}$ represent the overall heat fluxes from the $(i+1)^{th}$ layer to the i^{th} layer and to the i^{th} layer to the $(i-1)^{th}$ layer, respectively. A modified version of the conventional "layer by layer" model (McIntosh, 1994) is used to calculate the overall heat flux between two adjacent layers ($q_{rl,i}$). This is calculated as the sum of three different heat transfer mechanisms (see Eq. 6 in Table 2). The first mechanism considered for heat transfer is thermal radiation between each radiative layer (q_{rad}, Eq. 7 in Table 2). The second is the heat conduction through the solid spacer material ($q_{s,cond}$, Eq. 8 in Table 2). The last mechanism considered is the heat transfer through the gas ($q_{g,i}$, Eq. 9 in Table 2), which depends on the value of the Grashof number (*Gr*) as defined by Eq. 10 (where *g* is the gravitational acceleration, α is the coefficient of volume expansion, ΔT is the temperature difference between two adjacent layers, D_x is spacer thickness, ν is the kinematic viscosity of the gas). Conduction is the prevalent mechanism when $Gr < 2860$ (Xie et al., 2010), while convection prevails when $Gr \geq 2860$. In the first case, $q_{g,i}$ is expressed using the Sherman-Less relation (Sherman, 1963; Less and Liu, 1961). In the latter case, the value of the Nusselt number (*Nu*) for the calculation of the convective term (Eq. 13 in Table 2) depends on the Rayleigh number (*Ra*, namely the product *Gr•Pr*) as reported in Eq. 14 (Xie et al., 2010), where *Pr* is the Prandtl number (see Eq. 15 in Table 2, where μ is the dynamic viscosity of the gas, δ is the thickness of the enclosure between two layers, and H represents the longitudinal characteristic dimension of the enclosure). This layered approach to the calculation of the gas heat transfer contribution ($q_{g,i}$), based on the introduction of the Sherman-Less relation for conduction and on the switch to convection for high *Gr* and *Ra*, ensures the validity of the model over the entire range of pressures, from high-vacuum to atmospheric conditions (American Society for Testing and Materials, 2019). The approach allows to apply the model in all relevant pressure ranges, varying from normal operating conditions ($1.33 \cdot 10^{-4}$ to 1.33 Pa, according to American Society for Testing and Materials, 2019) to partial/complete loss of vacuum as observed in the fire tests by Wingerden et al. (2022). This represents an important improvement with respect to the model proposed by McIntosh (1994), which was limited to high-vacuum applications. However, it must be remarked that, as discussed in Section 7, the proposed approach is based on using the pressure within the insulation system as an input to the heat transfer model, and is not able to predict the pressurization in the gap during fire exposure deriving from the thermal decomposition of the MLI and the possible condensation of the evolved gaseous thermal degradation products.

The heat balance equations for the innermost (node *1*) and the outermost (node *N*) layers present some differences with respect to the other nodes. In the first case (Eq. 4 in Table 2), the radiative term of $q_{rl,1}$ takes into account the emissivity of the inner shell surface material. In the second one (Eq. 2 in Table 2), the heat transfer with the external wall (node S_e) is considered to occur by thermal radiation only. This is because a gap with no spacer is present between the N-th and the S_e nodes, so that the conduction and convection mechanisms are negligible in vacuum conditions.

Finally, Eqs. 1 and 5 in Table 2 represent the energy balance for the external and internal shell nodes, respectively. The term q_f is the external fire heat flux entering the outer tank wall and is the result of the contribution of radiative and convective heat transfer from the flame (ISO 21843, 2023) while q_L is the heat flux from the internal shell to the tank lading, which is governed by the convective heat transfer coefficient in the cryogenic fluid wetting the wall.

A further novelty with respect to the layer-by-layer model of McIntosh (1994) is that the high-temperature thermal degradation of MLI is taken into account by varying both the relative density (f_i) of the i^{th} spacer to the solid spacer material and the layer thickness ($\delta_{rl,i}$) as functions of the solid material mass loss (Eqs. 17 and 18 in Table 2).

The terms f_0 and $\delta_{rl,0}$ represent the initial nominal values of f_i and $\delta_{rl,i}$, respectively. The sample residual fraction, $Y_{s,i}$, is defined by Eq. 16 in Table 2 and represents the residual mass of the i^{th} layer ($m_{s,i}$) normalized to its initial value ($m_{s,0}$). The sample residual fraction decreases during TG runs according to the apparent kinetic described by Eq. 19 in Table 2 (at the starting point of the run, $Y_{s,i}$ equals 1). In Eq. 19, *n* is the apparent reaction order, *A* is the preexponential factor, E_a is the apparent activation energy, and *R* is the ideal gas constant. The values of the apparent kinetic parameters *n, A and* E_a were estimated on the basis of TG results. Following the method proposed by Şenocak et al. (2016), the estimation

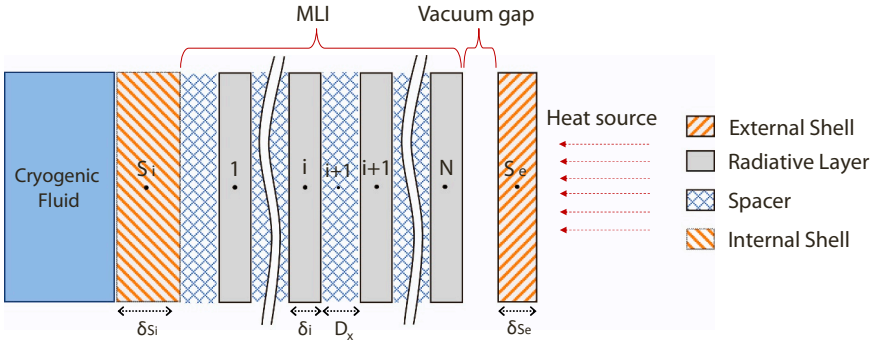

Fig. 4. Schematic representation of the thermal node discretization adopted to describe the heat transfer problem. S_e = external shell, S_i = internal shell. Nodes 1 to N refer to the MLI radiative layers.

Table 2
Equations used in the MLI degradation model. The symbols in the equations are defined in the nomenclature section (Num; equation number).

Node	Variable	Equation	Num.
S_e	T_{S_e}	$\delta_{S_e}\rho_{S_e}c_{p,S_e}\frac{dT_{S_e}}{dt} = q_f - \frac{1}{\left(\frac{1}{\varepsilon_{S_e}}+\frac{1}{\varepsilon_N}-1\right)}\sigma\left(T_{S_e}^4 - T_N^4\right)$	(1)
N	T_N	$\delta_{rl,N}\rho_{rl}c_{p,rl}\frac{dT_N}{dt} = \frac{1}{\left(\frac{1}{\varepsilon_{S_e}}+\frac{1}{\varepsilon_N}-1\right)}\sigma\left(T_{S_e}^4 - T_N^4\right) - q_{rl,N}$	(2)
i	T_i	$\delta_{rl,i}\rho_{rl}c_{p,rl}\frac{dT_i}{dt} = q_{rl,i+1} - q_{rl,i}$	(3)
1	T_1	$\delta_{rl,1}\rho_{rl}c_{p,rl}\frac{dT_1}{dt} = q_{rl,2} - q_{rl,1}$	(4)
S_i	T_{S_i}	$\delta_{S_i}\rho_{S_i}c_{p,S_i}\frac{dT_{S_i}}{dt} = q_{rl,1} - q_L$	(5)
-	$q_{rl,i}$	$q_{rl,i} = q_{rad,i} + q_{s.cond,i} + q_{g,i}$	(6)
-	$q_{rad,i}$	$q_{rad,i} = \frac{\sigma}{\left(\frac{1}{\varepsilon_i}+\frac{1}{\varepsilon_{i-1}}-1\right)}\left(T_i^4 - T_{i-1}^4\right)$	(7)
-	$q_{s.cond,i}$	$q_{s.cond,i} = \frac{C_2 f_i k_s}{D_x}\left(T_i - T_{i-1}\right)$	(8)
-	$q_{g,i}$	$q_{g,i} = \begin{cases} q_{g.cond,i} if\ Gr < 2860 \\ q_{g.conv,i} if\ Gr \geq 2860 \end{cases}$	(9)
-	Gr	$Gr = \frac{g\alpha\Delta T {D_x}^3}{\nu^2}$	(10)
-	$q_{g.cond,i}$	$q_{g.cond,i} = \left[\frac{D_x}{k_g} + \frac{2-\theta}{\theta}\cdot\frac{\sqrt{\frac{\pi MT}{2R}}}{\left(1+\frac{\zeta}{4}\right)P}\right]^{-1}\left(T_i - T_{i-1}\right)$	(11)
-	$q_{g.conv,i}$	$q_{g.conv,i} = Nu\frac{k_g}{D_x}\left(T_i - T_{i-1}\right)$	(12)
-	Nu	$\begin{cases} Nu = 0.197(Ra)^{1/4}\left(\frac{\delta}{H}\right)^{1/9}, 2\times10^3 < Ra < 2\times10^5 \\ Nu = 0.073(Ra)^{1/3}\left(\frac{\delta}{H}\right)^{1/9}, 2\times10^5 < Ra < 1.1\times10^7 \end{cases}$	(13)
-	Ra	$Ra = Gr{\cdot}Pr$	(14)
-	Pr	$\mathrm{Pr} = \frac{\mu c_{p,g}}{k_g}$	(15)
-	$Y_{s,i}$	$Y_{s,i} = m_{s,i}/m_{s,0}$	(16)
-	f_i	$f_i = f_0{\cdot}Y_{s,i}$	(17)
-	$\delta_{rl,i}$	$\delta_{rl,i} = \delta_{rl,0}{\cdot}Y_{s,i}$	(18)
-	$E_a; A; n$	$\frac{\mathrm{d}Y_{s,i}}{\mathrm{d}t} = -A\exp\left(-\frac{E_a}{RT_i}\right)\left(Y_{s,i}\right)^n$	(19)
		$\ln\left(\beta\frac{d(1-Y_S)}{dT}\right) = \ln(A) - \frac{E_a}{RT} + n{\cdot}\ln(Y_S)$	(20)

procedure was performed by a multilinear regression of the experimental data based on Eq. 20 in Table 2 (i.e., the linearized form of Eq. 19), where β is the heating rate.

The kinetic model represented by Eq. 19 in Table 2 is solved at each time step for all the MLI layers to calculate the value of $Y_{s,i}$ and update f_i and $\delta_{rl,i}$ until a specific threshold value $Y_{s,T}$ is reached (see Section 5.1). When the threshold value of the residual mass fraction is achieved, the i^{th} layer (both the radiation layer and the spacer) is considered to be completely degraded and is removed from the simulation. In the following time step, the energy balance for the $(i\text{-}1)^{th}$ layer is replaced by Eq. 2. Thus, the model simulates the gradual degradation of the MLI system.

4.2. Simulation cases for HTTVC test

The model introduced in Section 4.1 was used to simulate the HTTVC tests described in Section 3.3 in order to compare its prediction to the experimental results. The thermal node discretization presented in Section 4.1 was adapted to match the specific features of the experimental device. Node S_e (Fig. 4) was assigned to the bottom wall of the HTTVC, while node S_i was associated with the austenitic-steel-coated copper surface of the heat exchanger. Since the temperature of the bottom wall (T_{Se}) was directly measured during the test, its value over time was superimposed in the model simulation, thus not solving the thermal balance for node S_e. The same applies to node S_i, whose temperature (T_{Si}) was fixed at 4 °C, which corresponds to the initial temperature of the water inside the heat exchanger in both TEST #1 and TEST #2 (see Section 3.3). Although this increased during the tests (i.e., up to 26 °C), its variation from the initial value was disregarded in the model simulation for the sake of simplicity, as it did not significantly affect the value of the heat flux entering from the bottom wall.

Since the MLI is not in contact with the heat exchanger surface in the HTTVC, in the heat flux term $q_{rl,1}$ in Eqs. 4 and 5 in Table 3 (see Section 4.1) only radiation is accounted for, thus neglecting gas and spacer conduction. The simulated heat flux through the inner wall is considered as the reference value to be compared with the heat flux to the heat exchanger measured in the test, thus neglecting the thermal resistances within the heat exchanger wall and the cooling fluid, as supported by previous studies on MLI systems (Martin and Hastings, 2001). The MLI system properties used in the calculation are listed in Table 1.

Table 3
External wall material properties.

Property	Symbol	Value	Unit of measure	Source
Thickness	δ_{Se}	0.003	m	-
Density	ρ_{Se}	7944	kg/m^3	(Key to Metals AG, 2023)
Heat capacity	cp_{Se}	500	J/(kg·K)	(Key to Metals AG, 2023)
Thermal conductivity	k_{Se}	15	W/(m·K)	(Key to Metals AG, 2023)
External emissivity	$\varepsilon_{Se,out}$	0.5	-	-
Fire convective heat transfer coefficient	h_{air}	10	W/(m^2·K)	-

The apparent kinetic parameters were estimated through regression of the TG data, as discussed in Sections 4.1 and 5.1, where the values used in the present simulation are reported.

Eberwein et al. (2023) observed that the emissivity of the heat exchanger and of the bottom wall (i.e., ε_{Se} and ε_{Si}, respectively) increased considerably during the HTTVC tests as a result of the accumulation of pyrolysis products from the MLI (Eberwein et al., 2023). A white coating appeared during tests on the inner wall and a black coating formed at the bottom wall in contact with the system heater. In order to consider this phenomenon in the heat transfer model accounting for its variability, two simulation cases were analyzed for each test:

Case A. Emissivity values of ε_{Se} and ε_{Si} are set to 0.27, which corresponds to the initial emissivity of both surfaces according to Paloposki and Liedquist (2005) and Eberwein et al. (2023).

Case B. Emissivity values of ε_{Si} and ε_{Se} are set to 1 and 0.44, respectively, which represent the emissivity values measured at the end of the tests (Eberwein et al., 2023).

The pressure profile measured by Eberwein et al. (2023) in the vacuum chamber (see Section 5.2) was used as an input to the model in each simulation run.

During the experimental tests, the degradation of the MLI was limited to the central region of the sample (due to border effects close to the perimeter of the sample, induced by the cooling heat shield). Although in normal operating conditions (i.e., in the absence of material deterioration) the heat transferred through the MLI can be considered homogeneous over the entire sample surface, this is not true when localized thermal degradation phenomena occur. Thus, starting from the measured value of the thermal power entering the heat exchanger in the HTTVC test, the heat flux curve to be compared with the model results was calculated according to Eq. 21:

$$\begin{cases} q_{\exp} = \dfrac{\dot{Q}_{\exp}}{A_t} & if \quad t \le t_{td} \\ q_{\exp} = \dfrac{\dot{Q}_{\exp}}{A_d} & if \quad t > t_{td} \end{cases} \tag{21}$$

where $\dot{Q}_{\exp}$ is the thermal power measured by the heat exchanger of the HTTVC, A_t is the total cross-sectional area of the MLI sample (i.e., 0.042 m^2; see Section 3.3), A_d is the measured value of the MLI degraded area, and t_{td} is the time at which the thermal degradation of the last MLI layer occurred. These are determined after each experimental test (as discussed in Section 5.2).

4.3. Case studies

The developed model was applied to test the performance of the polyester-MLI system in full-scale test cases, simulating the behaviour of a double-walled tank filled with liquid hydrogen under realistic fire conditions. The MLI system was modelled according to the schematization presented in Fig. 4, assuming that the stored fluid is liquid hydrogen at atmospheric pressure. The scenario considered is a full engulfing fire and the heat flux entering the external wall of the tank, q_f, was computed according to Eqs. 22 to 24, where $q_{rad,f}$ and $q_{conv,f}$ are the fire radiative and convective heat fluxes, respectively, ε_f is the flame emissivity (here assumed equal to 1), T_f is the fire temperature, $\varepsilon_{Se,out}$ is the emissivity of the external wall on the side facing the fire, and h_f is the fire convective heat transfer coefficient.

$$q_f = q_{rad,f} + q_{conv,f} \tag{22}$$

$$q_{rad,f} = \sigma \varepsilon_{Se,out} (\varepsilon_f {T_f}^4 - {T_{Se}}^4) \tag{23}$$

$$q_{conv,f} = h_f (T_f - T_{Se}) \tag{24}$$

A set of four test cases was defined varying the fire temperature, T_f, according to four different standard curves:

- HCinc (DIN 1076:1999-11, 1999)
- HC (EN 1363–2 Part 2, 1999)
- ZTV-ING (BASt, 2015)
- ETK (ISO 834, 1999)

These standard fire curves are reported in national and international standards for the application to fire safety design in buildings, industrial equipment, and vehicles devoted to the transportation of dangerous goods (Blosfeld, 2009).

The material properties assumed were the same for each case study, considering AISI 316 L as the wall material for both the internal and external walls of the tank. The external wall properties used in the simulations are listed in Table 3, while the MLI properties are those reported in Table 1. The vacuum pressure was set to 10^{-3} Pa (as typical in MLI systems operating under high vacuum conditions). Possible loss of vacuum due to degradation was disregarded. The emissivity of the internal and external shell (on the side facing the MLI) were set to 1 and 0.44, respectively, thus considering the effect of MLI pyrolysis product solidification discussed in Section 4.2. The value of T_{Si} (see Fig. 4) was set to −253 °C, corresponding to the saturation temperature of liquid hydrogen at atmospheric pressure. This value was considered constant during the simulation for the sake of simplicity, as it did not significantly affect the value of the heat flux entering the inner wall of the tank.

The steady-state temperature profile obtained with $T_{Se} = 20$ °C was set as the initial condition through the MLI system.

With the aim of showing the importance of taking into account the MLI degradation, two additional case studies were defined for the "HCinc" fire scenario:

- HCinc_no_deg
- HCinc_no_MLI

In the case "HCinc_no_deg", it was assumed that the MLI never degrades during fire exposure, and the conventional layer-by-layer model as developed for normal operating conditions (McIntosh, 1994) was applied in the simulation.

In the "HCinc_no_MLI" case, the MLI is not present in the double wall of the tank and the simulation only considers the high vacuum between the two shells.

Both cases share the same external wall material properties listed in Table 3. The emissivity value, ε_{Si}, was assumed equal to the nominal value of 0.27, whereas ε_{Se} was set equal to 0.7 according to experimental measurements on AISI 316 L carried out by Balat-Pichelin et al. (2022) under vacuum and high-temperature conditions.

5. Results

5.1. Thermogravimetric (TG) analysis results

Fig. 5 shows some results obtained in the TG runs performed on the MLI and MLI components. Table 4 presents a systematic overview of the results obtained in all the TG runs carried out. As can be observed in Fig. 5a, reporting the residual weight loss the MLI in TG runs carried out at different heating rates, the residual mass fraction at the end of the TG runs in pure nitrogen (i.e., approximately 10% of the initial weight of the sample in the present analysis) is not influenced by the heating rate of the TG run in the range investigated.

The dTG curves for MLI and its components at a constant heating rate of 20 °C/min in pure nitrogen, presented in Fig. 5b, largely overlap, suggesting that the presence of the aluminium coating has no significant effects on the degradation mechanism of polyester. This behaviour is consistent across all the heating rates investigated (see Table 4).

As shown in Fig. 5c, comparing the results of TG runs at constant heating rate (20 °C/min) in 100% nitrogen and in air, when degradation

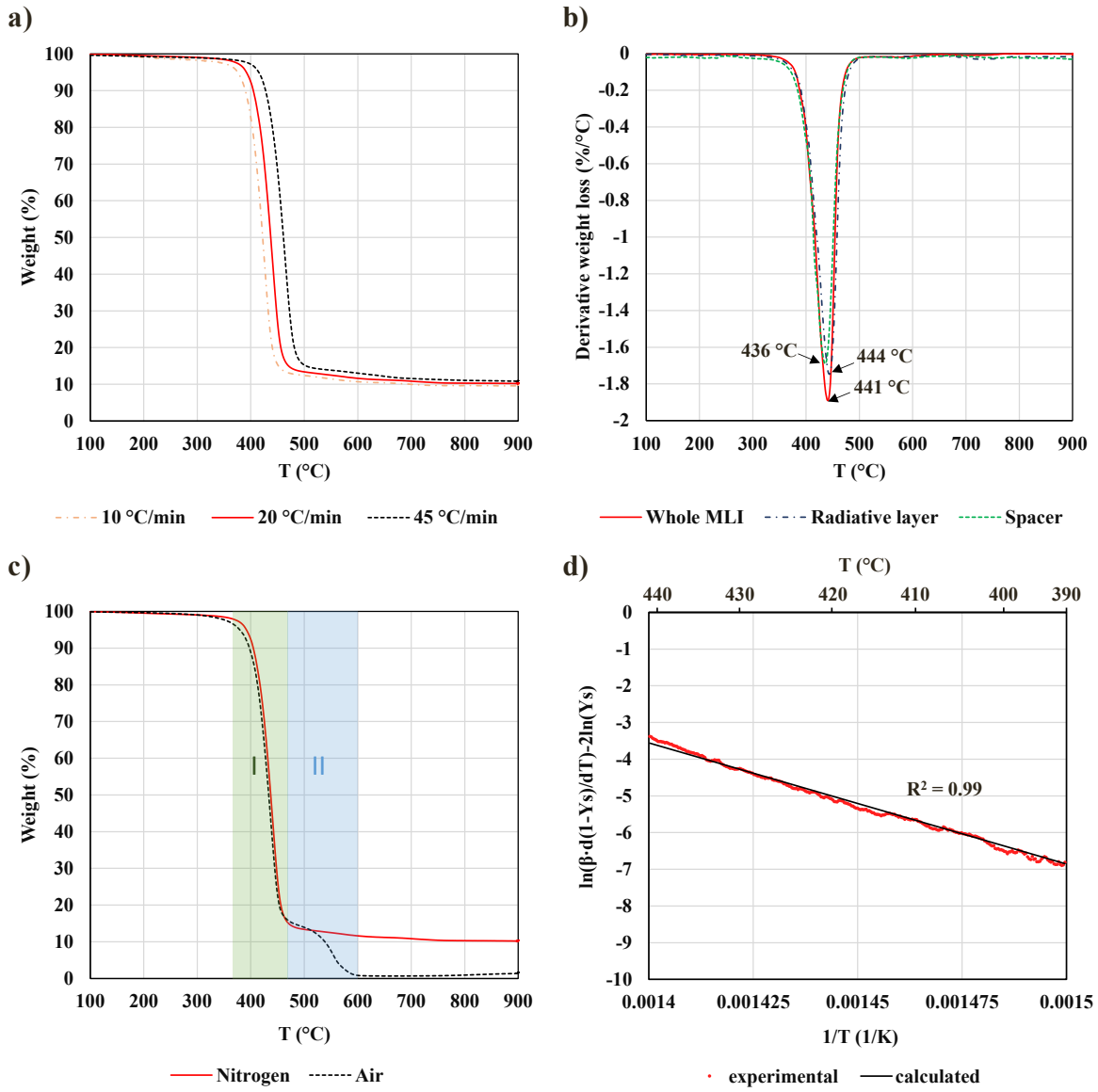

Fig. 5. Results of TG runs carried out on MLI samples: (a) MLI samples, weight loss with respect to temperature at constant heating rates between 10 and 45 °C/min in pure Nitrogen (100 mL/min); (b) dTG curves at constant heating rate (20 °C/min) for MLI and MLI components in pure nitrogen (100 mL/min); (c) TG curves at constant heating rate (20 °C/min) for MLI in pure nitrogen and air (100 mL/min); (d) kinetic analysis results for MLI sample at constant heating rate (20 °C/min) in pure nitrogen (100 mL/min) assuming an apparent second-order reaction (obtained using a multilinear regression of the experimental data, see Eq. 20 in Section 4.1).

occurs in a reactive atmosphere the TG curve shows a second region of degradation (shaded area **II** in Fig. 5c), in which the sample undergoes an almost complete decomposition to gaseous products.

The TG curve obtained at a constant heating rate of 20 °C in pure nitrogen was used to derive the apparent kinetic parameters of degradation as discussed in Section 4.1, according to the procedure presented by Şenocak et al. (2016). The following values for activation energy (E_a), pre-exponential factor (A), and reaction order (n) were obtained: A=3.22·10^{18} s^{-1}, E_a= 2.74·10^5 J/mol, n = 2. A coefficient of determination (R^2) of 0.99 was obtained. Fig. 5d shows the fit of the kinetic model to the experimental data.

The value of $Y_{s,T}$ (i.e., the value of the residual mass fraction, Y_s, at which the radiative layer is considered to be destroyed) was set to 0.161 (i.e. the residual fraction at the end of the degradation region, as shown in Table 4).

5.2. Model validation with HTTVC tests results

Fig. 6 shows the MLI in the sample carrier before (Figs. 6a and 6c) and after (Figs. 6b and 6d) the tests described in Section 3.3. The average value of the MLI degraded area, A_d, was obtained by pixel counting, resulting in 0.021 m^2 (approximately 50% of the initial sample surface area, A_t) and 0.019 m^2 (approximately 45% of A_t) for TEST #1 and TEST #2, respectively. The average value of t_{td} (i.e., the time at which all the MLI layers are degraded) was of 24 min and 0 s for TEST #1 and of 21 min 30 s for TEST #2. The times were determined on the bases of the sudden increase in the thermal power transferred to the heat exchanger (Eberwein et al., 2023).

Fig. 7 compares temperature and heat flow measured during the HTTVC tests with the simulation results of the MLI degradation model. In Figs. 7a and 7b, the continuous lines show the calculated temperature distribution of each radiative layer in Case B for TEST #1 and TEST #2, respectively (temperature curves for Case A, not shown for the sake of

Table 4
Temperature range and extension of weight losses for MLI and components in TG runs carried out at different heating rates and in different atmospheres.

Heating rate	Sample	100% Nitrogen		Air			
		Weight loss (%)	Temperature range (°C)	Weight loss Zone I (%)	Temperature range Zone I (°C)	Weight loss Zone II (%)	Temperature range Zone II (°C)
10 °C/min	MLI	80.7	360–470	77.8	370–450	12.4	450–540
	Polyester spacer	83.9	360–470	-	-	-	-
	Radiative layer	82.2	360–470	-	-	-	-
20 °C/min	**MLI**	**83.9**	**370–490**	**80.4**	**365–465**	**15.6**	**465–600**
	Polyester spacer	80.3	370–490	-	-	-	-
	Radiative layer	83.2	370–490	-	-	-	-
45 °C/min	MLI	83.0	390–510	82.2	360–480	10.7	480–615
	Polyester spacer	85.1	390–510	-	-	-	-
	Radiative layer	80.4	390–510	-	-	-	-

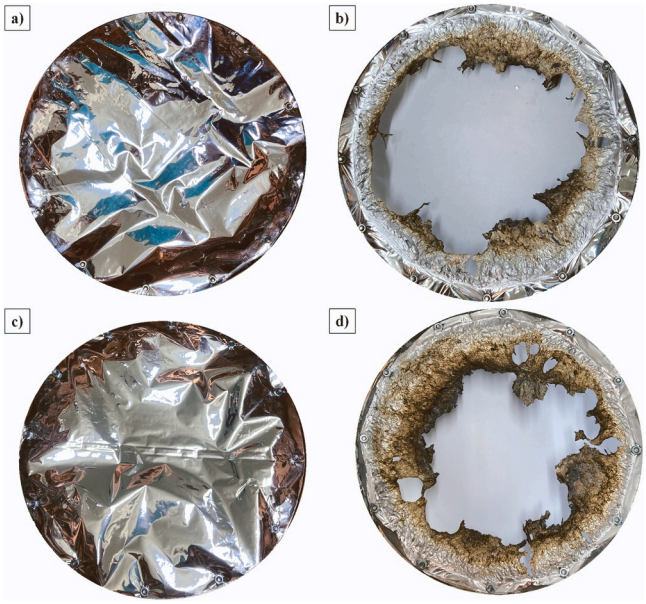

Fig. 6. Photos of the tested MLI on the sample carrier before (panels (a) and (c)) and after (panels (b) and (d)) the HTTVC test. Panels (a) and (b) refer to TEST #1 (maximum bottom wall temperature of 750 °C), while panels (c) and (d) refer to TEST #2 (maximum bottom temperature of 770 °C).

brevity, present a very similar behaviour). The dashed blue line refers to the bottom wall temperature (T_{Se}) measured in the tests, while the green dotted curve shows the pressure increment measured in the HTTVC, used as an input in the degradation model. Starting from 4 °C, the bottom heats up at a heating rate of 20 °C/min up to 750 °C for TEST #1 and 770 °C for TEST #2. As a result, the temperature of the radiative layers increases at a similar rate after an induction time of about 15 min. During the heating phase, each layer undergoes thermal degradation until its normalized residual mass reaches the threshold value $Y_{s,T}$, and the layer itself is removed from the simulation (see Section 4.1). This progresses until all the layers are degraded, in agreement with the experimental evidence (see Fig. 6).

When the higher heat flow intensity is considered (Case B) in the simulation run of TEST #1, the degradation of the first layer of the MLI facing the HTTVC (layer 10) is completed after 28 min 48 s, while the last layer (layer 1) is completely degraded after about 29 min 48 s. The bottom temperature (T_{Se}) when the degradation of the first layer of the MLI occurs is 590°C, while it corresponds to 615 °C when the last layer decomposes.

The calculated temperature distribution of the layers in the simulation of TEST #2 presents a similar behaviour (Fig. 7b). The thermal degradation of the MLI is anticipated of about 1 min compared to TEST #1 (29 min are necessary to complete the degradation of the last layer of the MLI). This is explained by the slightly higher heating rate of the bottom wall (21.2 °C/min for TEST #2 against 20 °C/min for TEST #1).

Figs. 7b and 7d compare the calculated values of the heat fluxes through the MLI obtained for the different emissivity values assumed in simulation Case A (dash-dotted line) and B (solid line) with the experimental data of TEST #1 and TEST #2, respectively (the details of the calculation procedure are reported in Section 4.2). In both tests, before the degradation effect is visible in the experiment (i.e., $t < t_d$), the difference in the wall emissivity for Cases A and B does not affect the calculated heat flux, since the radiative heat transfer process is controlled by the emissivity of the layers, not by that of the wall. As soon as all the MLI layers are degraded leaving the heat exchanger directly exposed to the hot bottom of the HTTVC, an abrupt increase in the heat flux (up to ~5 kW/m^2 for Cases A, and ~15.5 kW/m^2 for Case B) takes place. According to the model, this occurs respectively after 29 min 30 s and 29 min 48 s for Cases A and B in TEST #1, and after 29 min 0 s and 29 min 12 s in Cases A and B of TEST #2. The complete degradation of the MLI is predicted by the model respectively with a delay of about 6 and 8 minutes in the case of TEST #1 and TEST #2. A possible cause for this discrepancy is the shrinkage and embrittlement phenomena that affect the MLI sample during the tests, documented in Figs. 6b and 6d. Actually, such phenomena may induce fracturing of the radiative layers even before the thermal degradation process is completed (Eberwein et al., 2023).

Following the complete degradation of the MLI sample, the calculated heat flow curves increase to a steady state value (~9.5 kW/m^2 and ~10.7 kW/m^2 for simulation Case A of TEST #1 and #2 respectively, ~27 kW/m^2 and ~29.7 kW/m^2 for simulation Case B of TEST #1 and #2, respectively) that remains constant until the end of the run. During this stage the emissivity values considered in simulation Case A cause an underestimation of the measured heat flux, while the values used in Case B provide a better match with the experimental data. In particular, the maximum heat flux is slightly underestimated in simulation Case B, with an error of 4.3% in TEST #1 and of 4.7% in TEST #2 respectively. Therefore, the comparison between experimental and numerical results suggests that the change in wall emissivity due to the deposition of the pyrolysis products shall be taken into account to properly estimate heat flux through the degraded MLI system. The results of the simulation cases suggest that the use of the measured final wall emissivity values in model simulations provides satisfactory agreement with the experimental data. Therefore, as mentioned in Section 4.3, this value of

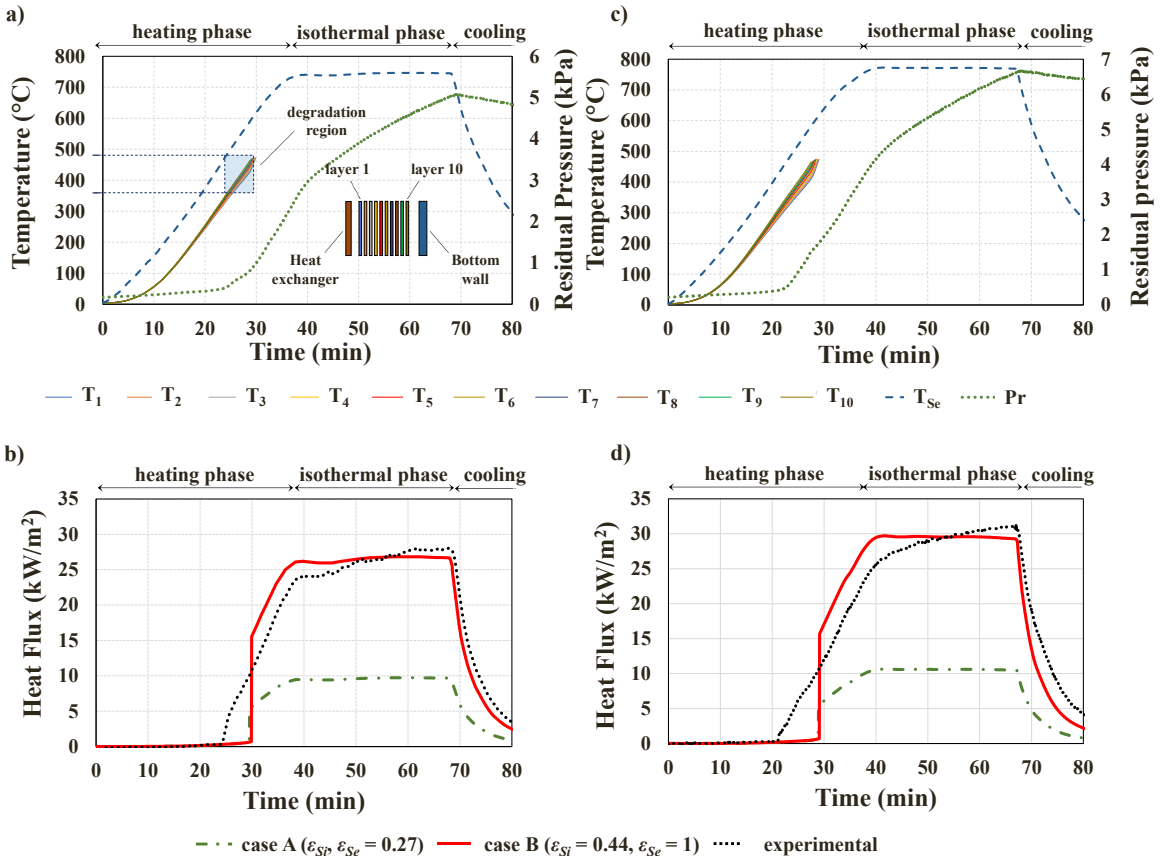

Fig. 7. Comparison between experimental and modeling results: (a) and (c) simulated temperature of the MLI radiative layers over time for Case B (continuous lines; layers 1 and 10 face the heat exchanger and the bottom wall of the HTTVC, respectively) compared with the measured HTTVC bottom temperature (dashed blue line) and pressure in the vacuum chamber (green dotted line) for TEST #1 (maximum bottom temperature of 750 °C) and #2 (maximum bottom temperature of 770 °C), respectively; (b) and (d) comparisons between the measured heat flow (black dotted line) towards the heat exchanger of the HTTVC and the simulated one for Case A (green dash-dotted line) and B (solid red line) for TEST #1 and TEST #2, respectively.

emissivity was considered when the model was applied in the full-scale case studies to assess the insulation performance of MLI systems for cryogenic tanks in external fire scenarios.

5.3. Results of the case studies

Fig. 8 shows the transient temperature evolution within the vessel insulation system obtained for the test cases described in Section 4.3.

The solid lines correspond to the simulated temperature of the radiative layers, while the dash-dotted lines show the temperatures of the external shell (T_{Se}) obtained for each fire standard curve. The fire temperature with respect to time postulated in each fire standard is represented by dashed lines in Fig. 8. The temperature of each MLI layer rises until the degradation is completed (i.e., $Y_s = Y_{s,T}$). It is evident how a faster increase in the fire temperature (T_f) corresponds to a shorter time required for the completion of the degradation of the MLI system. In particular, the fastest degradation process is observed for the "HCinc" case (i.e., the time required for the total degradation of the MLI, t_{td}, equals 3 min 12 s), followed by the "HC" fire curve (t_{td} = 4 min 18 s), and by the "ZTV-ING" fire curve (t_{td} = 5 min 12 s). The "ETK" case shows a significantly higher value of the time required for the total degradation of the MLI (t_{td} equals 11 min 30 s). The results in figure Fig. 8 highlight also that, when the i-th layer completes its degradation, the following one (i.e. the (i-1)-th layer) is suddenly exposed to the radiant heat from the external surface in contact with the fire and experiences a significant and rapid temperature increase.

The qualitative comparison of the temperature distributions in the MLI layers in Fig. 8 (high-vacuum conditions) with those obtained for higher pressures in the vacuum chamber reported in Section 5.2 (where the pressure is about 10^6 times higher) provides relevant information. The increased heat transfer, due to the presence of the gas, reduces the insulation performance of the single layers. Thus, the temperature distribution among the layers is more uniform (see Fig. 7) and those closer to the external wall of the tank are colder and resist for a longer time to the external fire.

Fig. 9 reports the calculated values of the heat flux through the inner wall of the tank (solid lines) and the postulated fire temperature (dashed lines) for each test case. The heat flux remains close to zero until the degradation temperature, t_{td}, is reached in the MLI layer farther from the outer vessel surface. When this temperature is reached, the last layer of the MLI degrades and an abrupt increase in the heat flux is observed for all the test cases. This indicates that, as long as at least one MLI layer resists, the tank lading is well insulated during fire exposure. However, when the last MLI layer fails leaving the inner shell of the vessel unprotected, the heat flux increases by 3 orders of magnitude, with values comprised between 16 and 73 kW/m^2 depending on the fire curve considered. Such values are high enough to induce fast pressurization and to threaten the integrity of the tank (Landucci et al., 2009).

Fig. 9a also reports a comparison of the heat fluxes resulting in disregarding MLI thermal degradation (case HCinc_no_deg) and not considering the presence of MLI (HCinc_no_MLI). In the first case, the heat flux increase is negligible over the entire simulation time. When the MLI is not present (case HCinc_no_MLI), the heat flux grows rapidly to the maximum value of 52 kW/m^2. However, the absence of thermal degradation phenomena affecting the inner wall emissivity due to the deposition of decomposition products (Eberwein et al., 2023) gives that

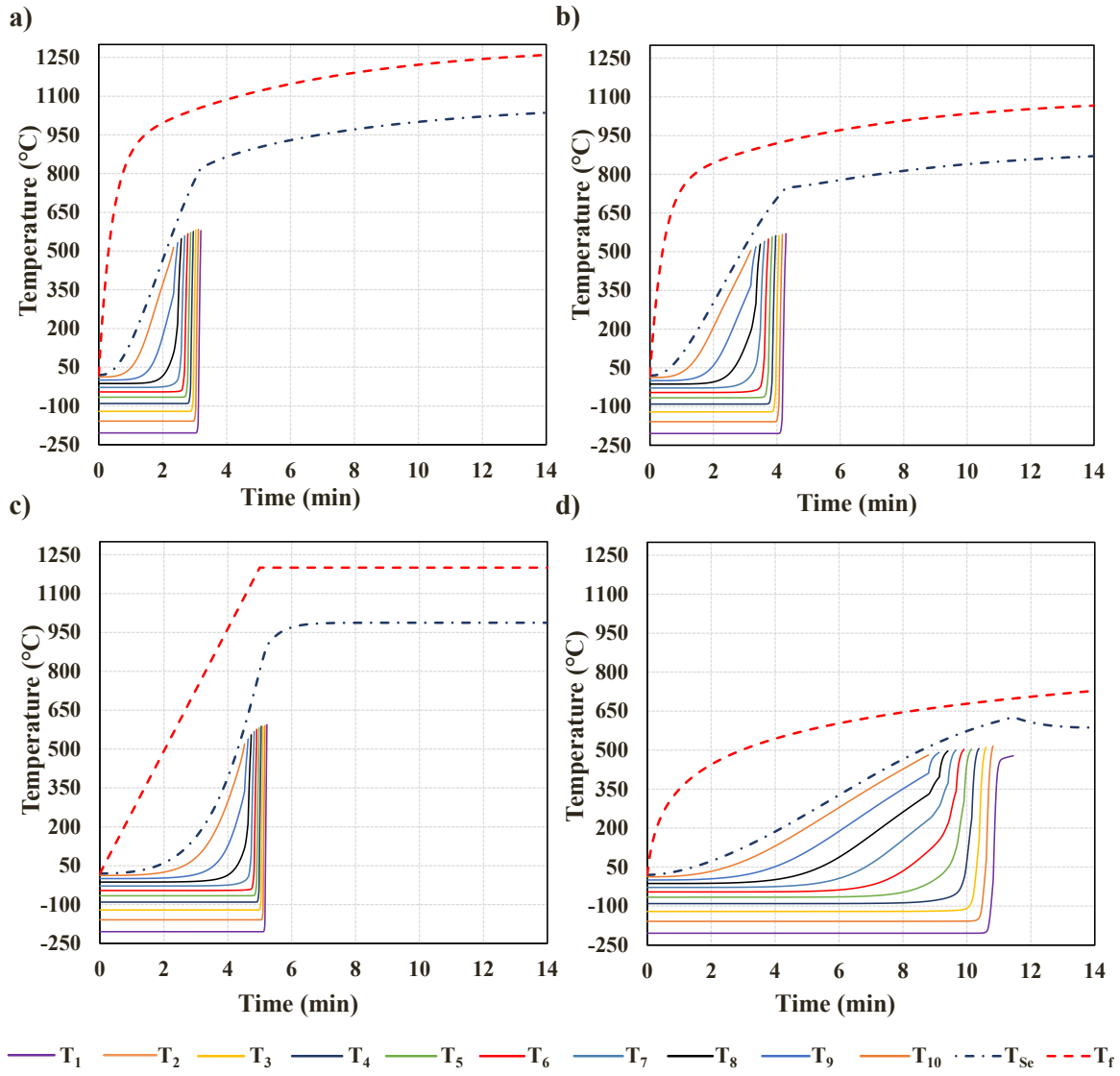

Fig. 8. Postulated fire temperature (T_f), calculated temperature of the external shell (T_{Se}) and model temperatures of the radiative layers over time considering different fire standards: HCinc (a), HC (b), ZTV-ING (c), ETK (d). A total of 10 radiation layers were considered in the model simulation. The number of each radiation layer corresponds to that in Fig. 4.

the maximum heat flux to the inner shell of the tank is lower than that obtained in the presence of MLI after the material degradation is completed (i.e. time higher than t_{td}). These results evidence that the presence of MLI may even have a negative effect in the case of an intense fire scenario, increasing the heat flux to the tank.

6. Discussion

The safety and asset integrity of tanks for the storage of cryogenic fluids pose several design challenges when the resistance to external fires is considered. In this context, exposure to external fire represents one of the most critical scenarios, that lies outside the range of applicability of the traditional approaches available in the literature to assess the performance and integrity of cryogenic tanks. The availability of models for the analysis of the performance of MLI-based thermal insulation systems is thus of paramount importance to assess the safety performance and the fire resistance of double-walled insulated cryogenic tanks. Models shall not only be able to simulate heat transfer in normal conditions but also to address system performance in abnormal conditions and/or in accident scenarios.

The innovative model developed proved to allow the straightforward assessment of the behaviour of MLI thermal insulation systems under fire exposure. Even if the present version of the model is not able to include the effects of layer shrinking, which are highly influenced by local material defects and by the specific set-up of the tank, the simulation of the HTTVC test data confirmed the model capability in predicting the MLI degradation dynamic and the evolution of the heat flux through the system in fire-like conditions.

It is worth remarking that, although it was applied to the specific MLI material described in Section 3.1 (aluminized-polyester radiative layers and polyester spacers), the proposed approach has general validity. In fact, upon detailed characterization of the thermal degradation kinetics, it may be used to simulate MLI systems based on different materials (e.g. aluminium-based MLI), and different geometries, such as variable density MLI (Wang et al., 2016). MLI systems combined with vapor-cooled shields (VCS) may also be simulated, provided that one (or more, depending on the type of system) thermal node is added to account for the energy sink represented by the VCS (Jiang et al., 2022).

When dealing with MLI exposure to fire, the loss of insulation performance due to the material degradation comes together with the generation of gaseous decomposition products in the vacuum jacket. Clearly enough, free convective heat transfer arises in such situations.

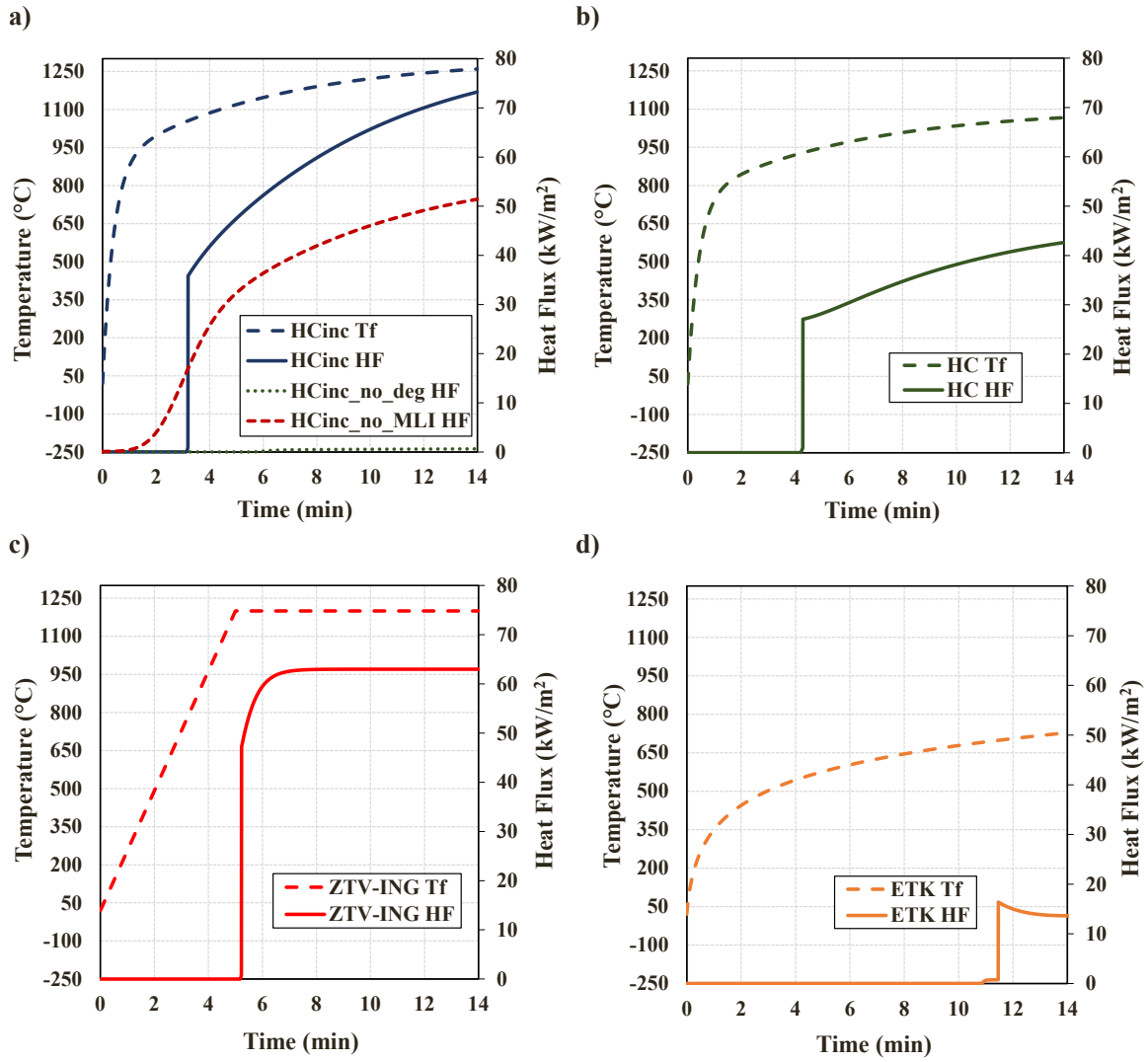

Fig. 9. Performance of MLI according to model simulation: heat flux through the inner wall of the tank over time (HF, solid lines) compared with the postulated fire temperature (T_F, dashed lines) for standards curves HCinc (a), HC (b), ZTV-ING (c), and ETK (d). Panel (a) also includes the heat fluxes calculated neglecting the presence of MLI (i.e., dashed red line, no_MLI_HF) and not accounting for MLI thermal degradation (green dotted line, no_DEG_HF).

On the one hand, this increases the heat fluxes compared to the case when only radiation is present (i.e. when high-vacuum is preserved). On the other, the enhanced heat transfer due to the presence of the gas decreases the temperature difference among the layers, providing a local cooling effect that could delay the thermal decomposition of the MLI materials with respect to the high-vacuum pressure cases. Further experiments and modeling activities are currently ongoing to quantify this effect. Nevertheless, it should also be remarked that the low temperature of the inner wall of the jacket may cause the gaseous decomposition to condense and/or frost, thus limiting the increase of the jacket pressure.

The results of model application to realistic fire scenarios involving the polyester-based systems for cryogenic liquid hydrogen tanks show that the MLI provides relevant protection only for a few minutes (up to 11 minutes in the simulations carried out) since the start of the fire. The MLI then degrades rapidly, exposing the tank to a high heat flux. The deposition of a layer of pyrolysis products onto the cold inner surface of the tank causes a change in emissivity that may even increase the heat flux with respect to the case where no MLI is present. All in all, the outcome of the study highlights the need to explore alternatives to MLI as a thermal insulation system for cryogenic liquid hydrogen tanks and suggests considering specific protections from external fires, as the application of fireproofing.

The innovative model obtained allows introducing a validated and physically sound approach to define the thermal boundary conditions. Moreover, the improved quantification of the thermal load supports the development of detailed models addressing the analysis of mechanical stresses and the calculation of the time to failure of cryogenic vessels exposed to fire. The model may thus be integrated into detailed models, either addressing the heat flow in thermal insulation jackets of cryogenic vessels or their mechanical integrity when exposed to external fires.

The results obtained also highlight the importance of investigating the performance of MLI systems when cryogenic vessels are involved in external fires. Actually, the developed model provides preliminary data to design mitigation systems aimed at preventing or delaying vessel failure and to support the management of emergency response.

7. Simplifying assumptions and limitations of the model

The present section summarizes the main simplifying assumption introduced in the modeling setup and discusses the limitations of the proposed approach.

The first important assumption is the choice of a 1-dimensional (1D) approach, which is widely adopted in the literature for the analysis of heat transfer in MLI systems (e.g., Jiang et al., 2021; McIntosh, 1994).

Although 3D effects might become important when considering full-scale applications, this simplification is reasonable for the purpose of developing a fundamental model as the one presented here. The validation against experimental results obtained with a setup that minimizes border effects demonstrates that the model can reasonably predict the degradation process of MLI and provide a reliable estimation of the maximum heat flux through the MLI system. This is an important and original result since the main purpose of the present approach is to provide a tool for the assessment of cryogenic tank safety. Clearly enough, the accurate simulation of scenarios involving non-uniform fire exposure conditions can only be achieved by extending the model to the second and third dimensions. However, the 1D approach can still be used to obtain a conservative assessment of the MLI performance.

The second main simplification concerns the mechanism of degradation, which is assumed to be only governed by the pyrolysis of the MLI components. The possible formation of fractures induced by mechanical stresses due to shrinkage effects was neglected. The outcome of the validation step suggests that this could anticipate by a few tens of seconds the thermal decomposition of the material, causing a local failure of the MLI. However, the phenomena involved in this early failure mechanism are strongly affected by the local stress and strain distribution, which in turn depends on the specific geometry of the system (i.e. its installation and anchoring to the tank wall). The formation of fractures and their propagation is also correlated to the presence of defects and local material inhomogeneities (Anderson and Anderson, 2005; Li et al., 2011). Thus, the simulation of this process is challenging, case-specific, and can only be attempted by finite element analysis (e.g., Nakamura and Kamath, 1992; He et al., 2020). This is out of the scope of the present study since it falls outside the aim of providing a general approach to MLI performance modelling in the case of external fires.

It is also important to highlight the effect of the loss of vacuum in the system, which plays an important role in the deterioration of thermal insulation performance. The model was designed to account for the pressure effect on the heat transfer rate, allowing for the simulation of scenarios characterized by any pressure value, from high-vacuum to atmospheric conditions. However, the pressure within the insulation system is an input to the model developed, which is not able to predict the pressure evolution in a jacket considering the generation of gaseous thermal degradation products and their possible condensation on the cold wall. In particular, the latter phenomenon is also strongly dependent on local geometry and specific conditions in the jacket (temperature of the inner wall, volume, etc.).

8. Conclusions

An innovative heat transfer model was developed to assess the behaviour of MLI under fire exposure conditions. The model includes MLI thermal degradation apparent kinetic parameters obtained from TG data. Experimental data obtained in a specifically designed device (the HTTVC) were used to assess the model capability of reproducing the degradation behaviour of MLI systems. The proposed approach can be extended to the simulation of other typologies of MLI-based thermal insulation systems, such as aluminium-based MLI, variable density MLI and MLI coupled with VCS systems upon characterization of the material apparent degradation kinetics.

The results of the model application for the assessment of the performance of polyester-based MLI systems for liquid hydrogen tanks in realistic fire scenarios provided relevant information concerning the vulnerability of cryogenic tanks in fire scenarios. In the case studies analyzed, all the fire scenarios ended with the complete degradation of the MLI after a short time-lapse, ranging between 198 s and 690 s. This confirms the importance of taking into account the deterioration of MLI thermal insulation performance in the case of a fire.

The outcome of the analysis based on standard fire curves points out the need for further research on MLI systems vulnerability to external fires. In this framework, the proposed approach may provide preliminary data to support emergency response management and can be used to define mitigation measures to protect the integrity of cryogenic tanks. Furthermore, the model is suitable to be integrated into CFD and lumped approaches for the simulation of the behaviour of cryogenic tanks in fire scenarios. Actually, the model developed overcomes the need for the empirical adjustment of the effective conductivity of the insulation system in detailed models. A validated physically sound approach is introduced to define the thermal boundary conditions. Likewise, the model can provide an improved quantification of the thermal load in detailed models addressing mechanical stress analysis for the calculation of time to failures of cryogenic vessels exposed to fire. All in all, the present approach paves the way to an improved detailed modelling and dynamic simulation of the behaviour of cryogenic tanks exposed to external fires.

CRediT authorship contribution statement

Valerio Cozzani: Supervision, Writing – original draft, Writing – review & editing, Conceptualization, Methodology. **Frank Otremba:** Data curation, Investigation. **Robert Eberwein:** Data curation, Investigation, Methodology. **Aliasghar Hajhariri:** Investigation, Data curation. **Carmela Chianese:** Data curation, Investigation, Methodology. **Giordano Emrys Scarponi:** Conceptualization, Investigation, Methodology, Writing – original draft. **Davide Camplese:** Conceptualization, Data curation, Investigation, Methodology, Writing – original draft.

Declaration of Competing Interest

The authors declare that they have no known competing financial interests or personal relationships that could have appeared to influence the work reported in this paper.

Acknowledgments

Funding received from the Italian Ministry of University and Research under the National Recovery and Resilience Plan, Mission 4, Component 2, Investment 1.3, NextGenerationEU, Project “Network 4 Energy Sustainable Transition”, PE00000021, CUPJ33C22002890007 is gratefully acknowledged.

References

Abbasi, T., Abbasi, S.A., 2007. The boiling liquid expanding vapour explosion (BLEVE): Mechanism, consequence assessment, management. J. Hazard. Mater. 141, 489–519. https://doi.org/10.1016/j.jhazmat.2006.09.056.

American Society for Testing and Materials, 2019. Standard Guide for Evacuated Reflective Insulation In Cryogenic Service (ASTM C740/740M-13).

Anderson, Ted L., Anderson, T.L., 2005. Fracture Mechanics, Third Edit. ed. CRC Press. https://doi.org/10.1201/9781420058215.

Aursand, E., Hammer, M., 2018. Predicting triggering and consequence of delayed LNG RPT. J. Loss Prev. Process Ind. 55, 124–133. https://doi.org/10.1016/j.jlp.2018.06.001.

Balat-Pichelin, M., Sans, J.L., Bêche, E., 2022. Spectral directional and total hemispherical emissivity of virgin and oxidized 316L stainless steel from 1000 to 1650 K. Infrared Phys. Technol. 123 https://doi.org/10.1016/j.infrared.2022.104156.

Bamford, C.H., Jenkins, A.D., 1955. Termination Reaction in Vinyl Polymerization: Preparation of Block Copolymers. Nature 176, 78. https://doi.org/10.1038/176078a0.

Bapat, S.L., Narayankhedkar, K.G., Lukose, T.P., 1990. Performance prediction of multilayer insulation. Cryog. (Guildf.) 30, 700–710. https://doi.org/10.1016/0011-2275(90)90234-4.

BASt (Bundesanstalt für Straßenwesen), 2015. Zusätzliche Technische Vertragsbedingungen und Richtlinien für Ingenieurbauten (ZTV-ING) Teil 5 “Tunnelbau” und Teil 3 “Massivbau”, Abschnitt 1 “Beton”.

Berge, G., 2009. Verification of VessFire. Petrell.

Blosfeld, J., 2009. Brandkurven für den baulichen Brandschutz von Straßentunneln, Berichte der Bundesanstalt für Straßenwesen, Reihe B: Brücken- und Ingenieurbau - 67.

Brown, T.C., Cederwall, R.T., Chan, S.T., Ermak, D.L., Koopman, R.P., Lamson, K.C., McClure, J.W., Morris, L.K., 1990. Falcon series data report: 1987 LNG vapor barrier verification field trials. Livermore, CA. https://doi.org/10.2172/6633087.

Corruccini, R.J., 1959. Gaseous heat conduction at low pressures and temperatures. Vacuum 7 19–29.
D'Aulisa, A., Tugnoli, A., Cozzani, V., Landucci, G., Birk, A.M., 2014. CFD modeling of LPG vessels under fire exposure conditions. AIChE J. 60, 4292–4305. https://doi.org/10.1002/aic.14599.
Dan, S., Lee, C.J., Park, J., Shin, D., Yoon, E.S., 2014. Quantitative risk analysis of fire and explosion on the top-side LNG-liquefaction process of LNG-FPSO. Process Saf. Environ. Prot. 92, 430–441. https://doi.org/10.1016/j.psep.2014.04.011.
Eberwein, R., 2021. Untersuchung der Gefährdung von Personen und Bauwerken in Folge des Versagens von LNG-Kraftstoffspeichern für Fahrzeuge in Tunneln. https://doi.org/10.14279/depositonce-11346.
Eberwein, R., Hajhariri, A., Camplese, D., Scarponi, G.E., Cozzani, V., Otremba, F., 2023. Insulation materials used in tanks for the storage of cryogenic fluids in fire scenarios, in: ASME 2023 Pressure Vessel and Piping Conference (PVP2023).
Edward, L., Filip, L., 2018. Influence of vacuum level on insulation thermal performance for LNG cryogenic road tankers, in: MATEC Web of Conferences. EDP Sciences, p. 1019.
European Committee for Standardization, 1999. Fire resistance tests—Part 2: alternative and additional procedures (EN 1363-2).
German Institute for Standardisation (Deutsches Institut für Normung) , 1999. Engineering Structures in Connection with Roads - Inspection and Test (DIN 1076: 1999-11).
Hadjisophocleous, G.V., Sousa, A.C.M., Venart, J.E.S., 1990. A study of the effect of the tank diameter on the thermal stratification in LPG tanks subjected to fire engulfment. J. Hazard. Mater. 25, 19–31. https://doi.org/10.1016/0304-3894(90)85067-D.
He, X., Larsen, R., Chen, F., Yin, H., 2020. Block cracking in surface coatings of polymeric substrates. Eng. Fract. Mech. 233, 107073 https://doi.org/10.1016/j.engfracmech.2020.107073.
Huang, Y., Wang, B., Zhou, S., Wu, J., Lei, G., Li, P., Sun, P., 2017. Modeling and experimental study on combination of foam and variable density multilayer insulation for cryogen storage. Energy 123, 487–498. https://doi.org/10.1016/j.energy.2017.01.147.
Hulsbosch-Dam, C., Atli-Veltin, B., Kamperveen, J., Velthuis, H., Reinders, J., Spruijt, M., Vredeveldt, L., 2017. Thermodynamic aspects of an LNG tank in fire and experimental validation. EPJ Web Conf. 143, 0–5. https://doi.org/10.1051/epjconf/201714302039.
Iannaccone, T., Landucci, G., Scarponi, G.E., Bonvicini, S., Cozzani, V., 2019. Inherent safety assessment of alternative technologies for LNG ships bunkering. Ocean Eng. 185, 100–114. https://doi.org/10.1016/j.oceaneng.2019.05.028.
Iannaccone, T., Scarponi, G.E., Landucci, G., Cozzani, V., 2021. Numerical simulation of LNG tanks exposed to fire. Process Saf. Environ. Prot. 149, 735–749. https://doi.org/10.1016/j.psep.2021.03.027.
International Organization for Standardization, 1999. Fire resistance tests (ISO Standard N. 834).
International Organization for Standardization, 2023. Determination of the resistance to hydrocarbon pool fires of fire protection materials and systems for pressure vessels (ISO Standard No. 21843:2023).
Ji, T., Zhang, R., Sunden, B., Xie, G., 2014. Investigation on thermal performance of high temperature multilayer insulations for hypersonic vehicles under aerodynamic heating condition. Appl. Therm. Eng. 70, 957–965. https://doi.org/10.1016/j.applthermaleng.2014.06.014.
Jiang, W., Sun, P., Li, P., Zuo, Z., Huang, Y., 2021. Transient thermal behavior of multilayer insulation coupled with vapor cooled shield used for liquid hydrogen storage tank. Energy 231, 120859. https://doi.org/10.1016/j.energy.2021.120859.
Jiang, W., Zuo, Z., Sun, P., Li, P., Huang, Y., 2022. Thermal analysis of coupled vapor-cooling-shield insulation for liquid hydrogen-oxygen pair storage. Int. J. Hydrog. Energy 47, 8000–8014. https://doi.org/10.1016/j.ijhydene.2021.12.103.
Johnson, M.R., 1998a. Tank car thermal analysis, user's manual for analysis program, Vol. 1. US Department of Transportation, Federal Railroad Administration, Washington DC.
Johnson, M.R., 1998b. Tank car thermal analysis, Technical Documentation Report for Analysis Program, Vol. 2. US Department of Transportation, Federal Railroad Administration, Washington DC.
Key to Metals AG, 2023. Total Materia - The world's most comprehensive Materials database [WWW Document]. URL https://portal.totalmateria.com (accessed 7.15.23).
Kunze, K., Kircher, O., 2012. Cryo-compressed hydrogen storage cryogenic cluster day. Oxford, Sept. 28, 2012.
Landucci, G., Gubinelli, G., Antonioni, G., Cozzani, V., 2009. The assessment of the damage probability of storage tanks in domino events triggered by fire. Accid. Anal. Prev. 41, 1206–1215. https://doi.org/10.1016/j.aap.2008.05.006.
Less, L., Liu, L., 1961. Kinetic theory description of plane compressible Couette flow, in: Proc. 2nd Int. Symp." on Rarefied Gas Dynamics", Academic Press.
Li, T., Zhang, Z., Michaux, B., 2011. Competing failure mechanisms of thin metal films on polymer substrates under tension. Theor. Appl. Mech. Lett. 1, 041002 https://doi.org/10.1063/2.1104102.
Martin, J.J., Hastings, L., 2001. Large-scale liquid hydrogen testing of variable density multilayer insulation with a foam substrate.
McIntosh, G.E., 1994. Layer by Layer MLI Calculation Using a Separated Mode Equation. In: Kittel, P. (Ed.), Advances in Cryogenic Engineering. Advances in Cryogenic Engineering. Springer US, Boston, MA, pp. 1683–1690. https://doi.org/10.1007/978-1-4615-2522-6_206.
Nakamura, T., Kamath, S.M., 1992. Three-dimensional effects in thin film fracture mechanics. Mech. Mater. 13, 67–77. https://doi.org/10.1016/0167-6636(92)90037-E.
NIST, 2019. NIST Chemistry WebBook 69, National Institute for Standards and Technology [WWW Document]. URL https://webbook.nist.gov/chemistry/ (accessed 7.11.23).
Paloposki, T., Liedquist, L., 2005. VTT Technical Research Centre of Finland. Steel emissivity High. Temp.
Pehr, K., 1996. Experimental Examinations on the Worst Case Behavior of LH2/LNG Tanks for Passenger Cars, in: Proceedings of the 11th World Hydrogen Energy Conference, Stuttgart, Germany. pp. 2169–2186.
Preuster, P., Alekseev, A., Wasserscheid, P., 2017. Hydrogen Storage Technologies for Future Energy Systems. Annu. Rev. Chem. Biomol. Eng. 8, 445–471. https://doi.org/10.1146/annurev-chembioeng-060816-101334.
Sánchez, A.L., Williams, F.A., 2014. Recent advances in understanding of flammability characteristics of hydrogen. Prog. Energy Combust. Sci. 41, 1–55. https://doi.org/10.1016/j.pecs.2013.10.002.
Scarponi, G.E., Landucci, G., Birk, A.M., Cozzani, V., 2019. An innovative three-dimensional approach for the simulation of pressure vessels exposed to fire. J. Loss Prev. Process Ind. 61, 160–173. https://doi.org/10.1016/j.jlp.2019.06.008.
Scarponi, G.E., Landucci, G., Ovidi, F., Cozzani, V., 2016. Lumped model for the assessment of the thermal and mechanical response of LNG tanks exposed to fire. Chem. Eng. Trans. 53, 307–312. https://doi.org/10.3303/CET1653052.
Şenocak, A., Alkan, C., Karadağ, A., 2016. Thermal Decomposition and a Kinetic Study of Poly(Para-Substituted Styrene)s. Am. J. Anal. Chem. 07, 246–253. https://doi.org/10.4236/ajac.2016.73021.
Sherman, F.S., 1963. A survey of experimental results and methods for the transition regime of rarefied gas dynamics. Rarefied Gas. Dyn. Vol. 2 (2), 228.
Speight, J., 2005. Lange's handbook of chemistry. McGraw-Hill Education.
Speirs, J., Balcombe, P., Blomerus, P., Stettler, M., Brandon, N., Hawkes, A., 2019. Can natural gas reduce emissions from transport. Heavy goods Veh. Shipp.
Sutheesh, P.M., Chollackal, A., 2018. Thermal performance of multilayer insulation: A review. IOP Conf. Ser. Mater. Sci. Eng. 396, 12061. https://doi.org/10.1088/1757-899X/396/1/012061.
Ustolin, F., Iannaccone, T., Cozzani, V., Jafarzadeh, S., Paltrinieri, N., 2021. Time to Failure Estimation of Cryogenic Liquefied Tanks Exposed to a Fire, in: Proceedings of the 31st European Safety and Reliability Conference (ESREL 2021). Research Publishing Services, Singapore, pp. 935–942. https://doi.org/10.3850/978-981-18-2016-8_182-cd.
Ustolin, F., Scarponi, G.E., Iannaccone, T., Cozzani, V., Paltrinieri, N., 2022. Cryogenic Hydrogen Storage Tanks Exposed to Fires: a CFD Study. Chem. Eng. Trans. 90, 535–540. https://doi.org/10.3303/CET2290090.
Van der Vegt, A.K., Govaert, L.E., 2003. Polymeren: van keten tot kunststof. DUP Blue Print.
Wang, B., Huang, Y.H., Li, P., Sun, P.J., Chen, Z.C., Wu, J.Y., 2016. Optimization of variable density multilayer insulation for cryogenic application and experimental validation. Cryog. (Guildf.) 80, 154–163. https://doi.org/10.1016/j.cryogenics.2016.10.006.
van Wingerden, K., Kluge, M., Habib, A.K., Skarsvåg, H.L., Ustolin, F., Paltrinieri, N., Odsæter, L.H., 2022a. Experimental Investigation into the Consequences of Release of Liquified Hydrogen onto and under Water. Chem. Eng. Trans. 90, 541–546. https://doi.org/10.3303/CET2290091.
van Wingerden, K., Kluge, M., Habib, A.K., Ustolin, F., Paltrinieri, N., 2022b. Medium-scale Tests to Investigate the Possibility and Effects of BLEVEs of Storage Vessels Containing Liquified Hydrogen. Chem. Eng. Trans. 90, 547–552. https://doi.org/10.3303/CET2290092.
Xie, G.F., Li, X.D., Wang, R.S., 2010. Study on the heat transfer of high-vacuum-multilayer-insulation tank after sudden, catastrophic loss of insulating vacuum. Cryog. (Guildf.) 50, 682–687. https://doi.org/10.1016/j.cryogenics.2010.06.020.
Zalosh, R., Weyandt, N., 2005. Hydrogen fuel tank fire exposure burst test. SAE Trans. 2338, 2343.